Science and Technology of Advanced Materials

ISSN: (Print) (Online) Journal homepage: www.tandfonline.com/journals/tsta20

Structural, mechanical, electronic and optical properties of N-decorated single-walled silicon carbide nanotube photocatalyst for hydrogen evolution via water splitting: a DFT study

Yahaya Saadu Itas, Razif Razali, Salisu Tata, Mohammed Kolo, Hamid Osman, Abubakr M. Idris & Mayeen Uddin Khandaker

To cite this article: Yahaya Saadu Itas, Razif Razali, Salisu Tata, Mohammed Kolo, Hamid Osman, Abubakr M. Idris & Mayeen Uddin Khandaker (2023) Structural, mechanical, electronic and optical properties of N-decorated single-walled silicon carbide nanotube photocatalyst for hydrogen evolution via water splitting: a DFT study, Science and Technology of Advanced Materials, 24:1, 2271912, DOI: 10.1080/14686996.2023.2271912

To link to this article: https://doi.org/10.1080/14686996.2023.2271912

Published online: 06 Nov 2023.

SCIENCE AND TECHNOLOGY OF ADVANCED MATERIALS
2023, VOL. 24, NO. 1, 2271912
https://doi.org/10.1080/14686996.2023.2271912

Taylor & Francis
Taylor & Francis Group

Structural, mechanical, electronic and optical properties of N-decorated single-walled silicon carbide nanotube photocatalyst for hydrogen evolution via water splitting: a DFT study

Yahaya Saadu Itas[a], Razif Razali[b], Salisu Tata[a], Mohammed Kolo[c], Hamid Osman[d], Abubakr M. Idris[e,f] and Mayeen Uddin Khandaker[g,h]

[a]Department of Physics, Bauchi State University Gadau, Bauchi, Nigeria;
[b]Department of Physics Faculty of Science, Universiti Teknologi Malaysia, Johor, Malaysia;
[c]Department of Physics, Borno State University, Maiduguri, Nigeria;
[d]Department of Radiological Sciences, College of Applied Medical Sciences, Taif University, Taif, Saudi Arabia;
[e]Department of Chemistry, College of Science, King Khalid University, Abha, Saudi Arabia;
[f]Research Center for Advanced Materials Science (RCAMS), King Khalid University, Abha, Saudi Arabia;
[g]Centre for Applied Physics and Radiation Technologies, School of Engineering and Technology, Sunway University, Bandar Sunway, Malaysia;
[h]Faculty of Graduate Studies, Daffodil International University, Dhaka, Bangladesh

ABSTRACT

This work investigates the fundamental photocatalytic properties of nitrogen-doped single-walled silicon carbide nanotubes (N-doped SWSiCNTs) for hydrogen evolution for the first time. Investigations of the structural, mechanical, electronic, and optical properties of the studied systems were carried out using popular density functional theory implemented in quantum ESPRESSO and Yambo codes. Analysis of the structural properties revealed high mechanical stability with the 3.6% and 7.4% N-doped SWSiCNT. The calculated band gap of the N-doped SWSiCNT with 3.6% demonstrated a value of 2.56 eV which is within the photocatalytic range of 2.3 eV–2.8 eV. The hydrogen evolution reaction (HER) and oxygen evolution reaction (OER) potentials of the 3.6% N-doped SWSiCNT also showed good agreement with previous theoretical data. The studied material showed the best photocatalytic performance in both parallel and perpendicular directions by absorbing photons in the visible region. Therefore, the observed structural, mechanical, electronic and optical behaviors demonstrated by the 3.6% N-doped SWSiCNT exposed it as a better photocatalyst for hydrogen production under visible light.

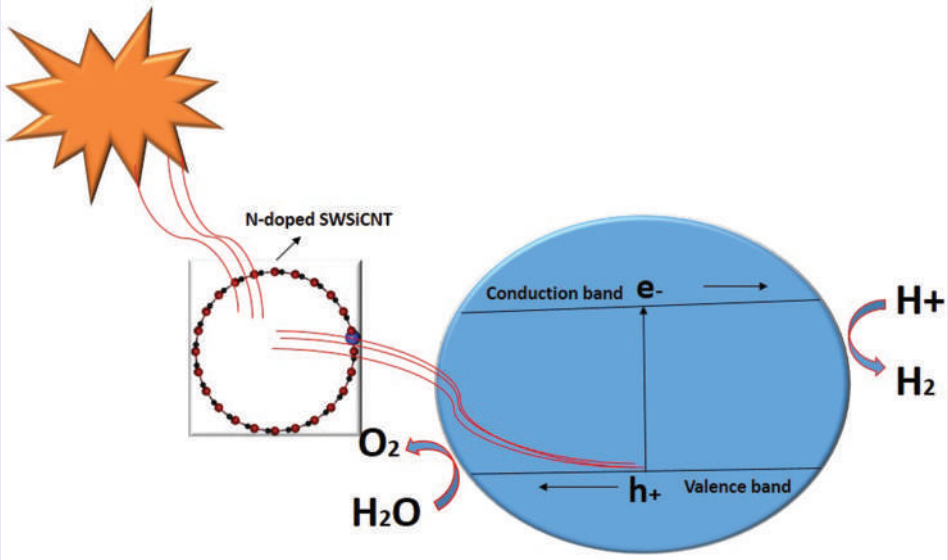

ARTICLE HISTORY
Received 6 September 2023
Revised 11 October 2023
Accepted 12 October 2023

KEYWORDS
Photocatalyst; silicon carbide nanotubes; water splitting; hydrogen energy

IMPACT STATEMENT

- This work reports fundamental photo-performance properties of a new system, i.e. nitrogen-doped single-walled silicon carbide nanotubes (N-doped SWSiCNTs) as photocatalysts for the overall water splitting for the first time. The observed structural, mechanical,

CONTACT Mayeen Uddin Khandaker mayeenk@sunway.edu.my; mu_khandaker@yahoo.com Centre for Applied Physics and Radiation Technologies, School of Engineering and Technology, Sunway University, Bandar Sunway, Selangor 47500, Malaysia

electronic and optical behaviors demonstrated by the N-doped SWSiCNT exposed it as a better photocatalyst for hydrogen production under visible light, indicating it to be a better candidate for photocatalytic applications such as water splitting, biodegradation, and wastewater purification.
- 3.6% N conc. has been found to be the suitable photocatalyst for water splitting.

1. Introduction

In recent decades, there have been reports of excessive usage of non-renewable energy, which has raised anticipation of a rapid end to this source of energy [1]. Global warming and climate change were also promoted due to the discharge of greenhouse gases through the use of fossil fuels [2]. Moreover, our ecosystems and waterbodies including surface waters were polluted and contaminated through this process [3]. These issues, along with others including the potential for depleting non-renewable energy sources, have led to the development of new ideas as fossil fuel alternatives, one of which is the production of hydrogen fuel and CO_2 reduction. It has been reported that CO_2 can be successfully reduced by tailoring the surfaces and interfaces of copper-based catalysts by electrochemical methods [4]. Zhang et al. also reported an efficient CO_2 reduction using a Cu-Zn – based alloy/oxide interface, which yields C^+ products [5]. Apart from CO_2 reduction, electrocatalysts were also found to take part in hydrogen evolution reactions in alkaline water [6]

The sun is the largest source of renewable energy, producing up to 1.23×10^{35} Joules of energy in 1 year, and many technologies have been harvested based on it to meet the global energy demand [7]. More specifically, to solve the ever-growing energy crisis and environmental problems, solar energy has been exploited through various means and many methods. Photocatalysis (i.e. light energy is used to drive chemical reactions) is one of the successful techniques that has evolved to make hydrogen energy as a possible replacement for fossil fuels [8].

Studies in the literature have demonstrated that H_2 and carbon-free fuel are possible perfect energy carriers because, when combined with O_2 in a fuel cell (FC), they only result in the production of water due to the chemical energy stored in the H–H bond [9]. However, several issues need to be addressed such as the problem of an efficient industrial-scale hydrogen development process [10], the problem of efficient large-scale storage facilities and the potential of the hydrogen capability to eliminate any waste products with a particular focus on carbon dioxide and other greenhouse gases [11]. Some of the processes that have been adopted for hydrogen production include biological, thermal-chemical, electrolytic, photocatalytic, and photo-electrolytic processes [12]. In the photocatalytic process, it was found that several materials serve as photocatalysts that successfully generate hydrogen throughout the water-splitting process. Recent findings revealed that nitrogen deficient Boron Nitride Nanotubes (BNNTs) performed better as photocatalysts in the decontamination of pollutants and hydrogen evolution due to minimum recombination of charge carriers [13].

Research conducted by Yuali et al. showed that the porosity of floury MoS_2 enhances its photocatalytic performance through adsorption and transfer of methylene blue (MB) to the active site [14]. However, this type of photocatalyst did not last long under strong sunlight and therefore needs to be improved. TiO_2 nanotubes have shown excellent performance against solar radiation in the visible range [15] and have been successfully used for water decontamination [16]. This property has been remarkably achieved due to its high surface area-to-volume ratio, high stability and favorable photoelectric property conversion characteristics. In a study conducted by Wang et al. (2019) reported that narrow band gap (2.6–2.8 eV) of $(Zn_{1+x}Ge)(N_2O_x)$ was the reason for its photocatalytic properties [17,18]. It has also been reported that doping sites significantly affect the photocatalytic activities of semiconductors [19].

In addition, other photocatalysts such as carbon nanotube composites, metal oxide nanotubes and so on have been tested for hydrogen evolution using water-splitting technology. The main problem is their ability to absorb large amounts of photons in the visible range, which depends on the electronic interactions between atoms in the valence bands and conduction bands [20]. During the generation of hydrogen by photocatalysts, photons with sufficient energy hit the semiconductor surface, which excites electrons into the conduction band. This leaves holes in the valence band whose interactions, along with those of the conduction band electrons, stimulate the absorption of electromagnetic energy from the Sun. Water splitting is the process in which hydrogen is evolved from the reduction reaction and the oxidation reaction of water molecules. The process is called Hydrogen Evolution Reaction (HER) and Oxygen Evolution Reaction (OER). The equations for total water splitting are given as [21]

$$4H^+ + 4e^- \rightarrow 2H_2 \text{ (hydrogen evolution)} \quad (1)$$

$$2H_2O \rightarrow O_2 + 4H^+ + 4e^- \text{ (oxygen evolution)} \quad (2)$$

Photocatalytic water splitting technology is a good technology that uses solar radiation to generate hydrogen from water and also helps provide clean energy sources. For a material to work well as a photocatalyst for water splitting, the range of the band gap should be between 2.2 eV and 2.8 eV and has to be more than the free energy of water splitting (1.23 eV) [22]; therefore, the energy of the photo-generated electrons must be greater than the 1.23 eV. In addition, it should absorb solar energy in the visible range. Also, the band gap should be less than 3.0 eV to prevent poor luminous efficiency, and the HER and OER potentials should be 0.02 eV and −0.77 eV, respectively [23]. To provide more materials (i.e. explore new materials) that are better suited for the production of hydrogen throughout the water-splitting process, this study investigated the mechanical, electronic, and optical properties of new photocatalysts optimized from nitrogen doping to single-walled (7, 7) silicon carbide nanotubes (SWSiCNT). It is worth mentioning that no other studies have been conducted previously on the photocatalytic properties of N-decorated single-walled silicon carbide nanotubes for the purpose of hydrogen evolution via the overall water-splitting technique. Additionally, we have been prompted to continue research in photocatalysts because of the diverse applications of photocatalytic processes in different fields. For instance, the practical applications of the photocatalytic process have already been demonstrated by many researchers worldwide, including Professor Santiago Esplugas, who has reported the significance of various photocatalysts in areas such as wastewater treatment, treatment of metoprolol, photooxidation, etc. [3,12].

2. Research method

The optimizations of the geometric structure of the nitrogen-doped SWSiCNT were performed using DFT with generalized gradient approximation (GGA) parameterized exchange-correlation and the Perdew – Burke–Ernzerhof (PBE) functional [24,25]. All calculations were performed using quantum ESPRESSO and Yambo codes [26]. Quantum ESPRESSO was chosen for this work because it is the leading high-performance open-source quantum mechanical software package for the nanoscale modeling of materials [27]. Due to some of its limitations such as band gap underestimations, we interface the quantum ESPRESSO with a Yambo hybrid soft code to obtain an accurate description of the investigated systems.

The optimized structure was visualized with VESTA and BURAI. As a representative model of our study, we considered the armchair shape of SWSiCNT with (7, 7) configurations having 28 atoms. The entire structure consists of alternating Si and C atoms separated by a bond length of 1.7 Å. To investigate the free hydrogen evolution reaction (HER) and the oxygen evolution reaction (OER), we adopted the technique [28] by Nrskov and coworkers, which was calculated using the following Equation (3),

$$\Delta G = \Delta E + \Delta ZPE - T\Delta S \quad (3)$$

where the terms ΔE, ΔZPE, ΔS and T denote the difference in total energy, zero potential energy, entropy and temperature (300 K), respectively. The graphical representation of the whole photocatalytic process is shown in Figure 1.

An optimized system of N-doped SWSiCNT was built such that the nitrogen impurity concentration in the pristine SWSiCNT was 3.6% and 7.4% under different dopings. To achieve a good agreement between computational cost and accuracy, we used a kinetic energy cutoff value of 60 Ry to perform all ground state computations on the basis set containing 1 × 1 × 30 sample k-points in the gamma point of the Brillouin zone. To determine the mechanical stability

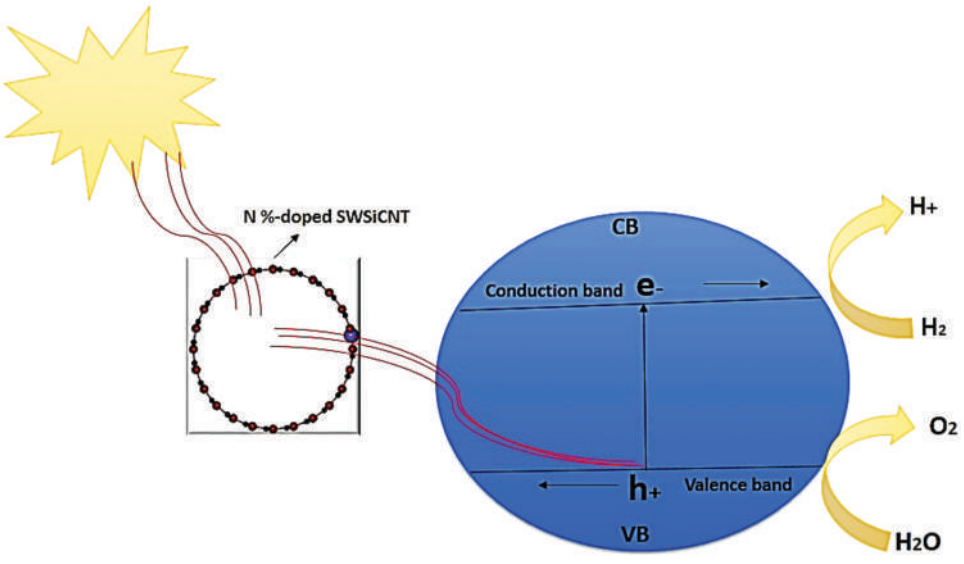

Figure 1. Graphical representation of the photocatalytic process of N-doped SWSiCNT.

of the pristine and N-doped systems of SWSiCNT, we used the given Murnaghan equation of state (shown in Equation (4)), which describes the relationship between the volume of the pristine and N-doped systems with the tensile pressure [29].

$$S(V) = \frac{K_0}{K_0'}\left[\left(\frac{V}{V_0}\right)^{-K_0'} - 1\right] \quad (4)$$

Where $\frac{V}{V_0}$ is the reduction in the volume of the nanotubes under stress and $\frac{K_0}{K_0'}$ is the reduction of the force constant under stress. In order to analyze the photocatalytic energy range of the pure and N-doped systems of SWSiCNTs, the electronic band gap and the total density of states were evaluated. Concerning the photo absorption properties of the systems, we determined the optical absorption energies of the studied systems using the imaginary dielectric functions based on the Kramers-Kronig relations, as shown in Equation (5) [30].

$$\varepsilon_2 = -\frac{2\omega}{\pi} P \int_0^{\infty} \frac{\varepsilon_1(\omega') - 1}{\omega'^2 - \omega^2} d\omega' \quad (5)$$

Where ω is real and where P denotes the Cauchy principal value.

3. Results and discussion

3.1 Structural and mechanical (elastic) properties

To study the photocatalytic properties of nanosystems, it is crucial to analyze their resistance to mechanical exposure to solar radiation. Photocatalysts with lower Young's moduli, low surface area to volume ratio, and low tensile stress are not efficient for photo absorption [31]. As part of this work, we have investigated the structural and elastic properties of the systems under investigation and analyzed the results accordingly. The optimized structure of the pristine SWSiCNTs, C-replaced N-doped SWSiCNTs and Si-replaced N-doped SWSiCNTs are shown in Figure 2(a–c), respectively, while Table 1 presents the distribution of formation energies with different states of the SWSiCNT systems. It can be seen from Table 1 that the diameter of the SWSiCNT decreased from 30.01 Å to 29.51 Å and 29.02 Å when 3.6 wt% and 7.4 wt% N dopants were used, respectively. This is because, with increasing tensile (external) pressure on the nanotube, its volume decreases. In the end, Si and C atoms are pressed together and bond lengths are shortened. Conversely, a decrease in the tensile pressure leads to an increase in the volume of the nanotube since the Si and C atoms are now far apart. In addition, the formation energy is highest for Pristine SWSiCNT and lowest for 7.4 wt% N-doped SWSiCNT. The claim to this statement rests on the fact that the release of energy for bond formation is always negative since this process is always exothermic. In addition, N dopants favored the N-doped SWSiCNT system via reduction of the formation energy of Si vacancies, hence affecting the charge transfer of neighboring atoms [32].

It was found that SWSiCNT was not stable when N atoms replaced the C atoms. However, the system showed good stability when N atoms in different concentrations were used to replace Si atoms which were in good accordance with the obtained experimental results [33]. The doping was done by replacing C atoms with N atoms in the original structure of (7, 7) SWSiCNT, giving the atomic composition of the doped system 50% Si, 46.4% C and 3.6% N atoms. The calculated bulk modulus for pristine SWSiCNT was 913.6 GPa, while that of the N-doped (7, 7) SWSiCNT was 929.4 GPa. The tensile pressure (strain) showed an inverse variation with volume for all nanotube systems, which is consistent with the obtained theoretical insights [34].

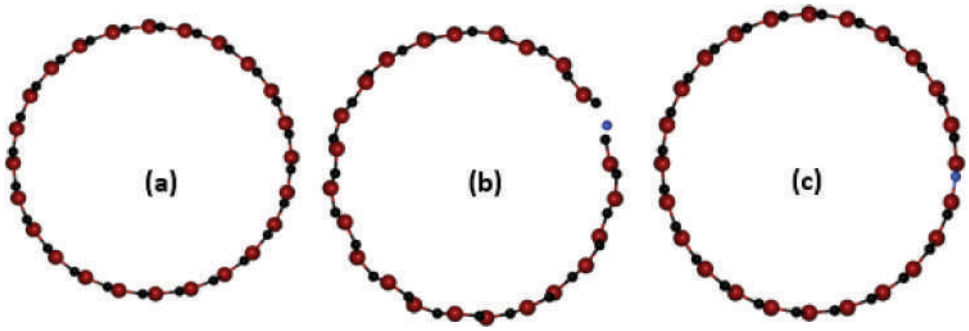

Figure 2. The optimized structures of (a) pristine SWSiCNT, (b) C replaced N-doped SWSiCNT and (c) Si replaced N-doped SWSiCNT.

Table 1. Formation energy distribution of the investigated systems.

Material	Substitution	Type of defect	Formation energy (eV)	Diameter (Å)
Pristine SWSiCNT	No substitution	No defect	12.34	30.01
3.6% N-doped SWSiCNT	N atoms replaced Si atoms	N_{Si}	10.36	29.51
7.4% N-doped SWSiCNT	N atoms replaced Si atoms	N_C	9.42	29.02

In the case of bare SWSiCNT, the most stable volume of the optimized nanotube corresponds to 1777.44 $(a.u)^3$ as shown in Figure 3(a). In this region, any additional increase in volume of the system will lead to severe defects such as dislocations. Figure 3(b) shows that the most stable volume of the 3.6% N-doped SWSiCNT is blue-shifted. This has happened due to N-doping following the reduced atomic radius of the N atom. Due to the increase in the concentration of the N-dopant from 3.6% to 7.14% (Figure 3(c)), the most stable volume further decreased to 1776.36 $(a.u)^3$. However, it should be noted that the calculated volumes of these nanotubes are still within the experimental range and therefore have not changed the mechanical stability of the systems studied. Figure 3(d) shows the effect of volume variation on the total energy of the pristine SWSiCNT system. It can be seen that the total energy varies directly and then inversely with the volume of the nanotube. The optimal volume required to achieve the overall optimized energy of the system was found to be 1283.91 $(a.u)^3$, which corresponds to a total energy of −985.35 eV. In this region, the electron–hole interactions outweigh the nucleus–nucleus interactions. The optimized volumes determined for 3.6% and 7.4% N-doped SiC nanotubes were 1283.82 $(a.u)^3$ and 1281.91 $(a.u)^3$, respectively. It was found that the obtained values for the optimized volumes of the N-doped systems all agreed well with the standard experimental data for nanotubes [35]. Furthermore, the calculated mechanical strength found from the N-doped SWSiCNT systems demonstrated their good ability to withstand much mechanical pressure during photo absorption.

To determine Young's modulus of the nanotubes under consideration, we have evaluated the total energy of both pristine and N-doped (7, 7) SWSiCNTs under different bond lengths using the pure DFT method. Results were obtained for variation of deformation energy with different Si-C and C-N bond lengths and the corresponding Young's modulus was obtained. Figure 4(a) presents the obtained results by varying bond lengths. From the results obtained, the closest distance between the two nearby Si-C atoms was 1.71 Å which corresponds to a bond energy of −985.35 eV. The previously obtained optimized volume of 1283.91 $(a.u)^3$ (shown in Figure 3(a)) is in good agreement with the obtained experimental values of 1.7 Å [36]. Figure 4(b,c) showed that the calculated bond lengths of the 3.6% and 7.4% N-doped SWSiCNTs were 1.69 Å and 1.68 Å, respectively. The lower value of the bond lengths of these nanotubes compared to pristine SWSiCNT makes

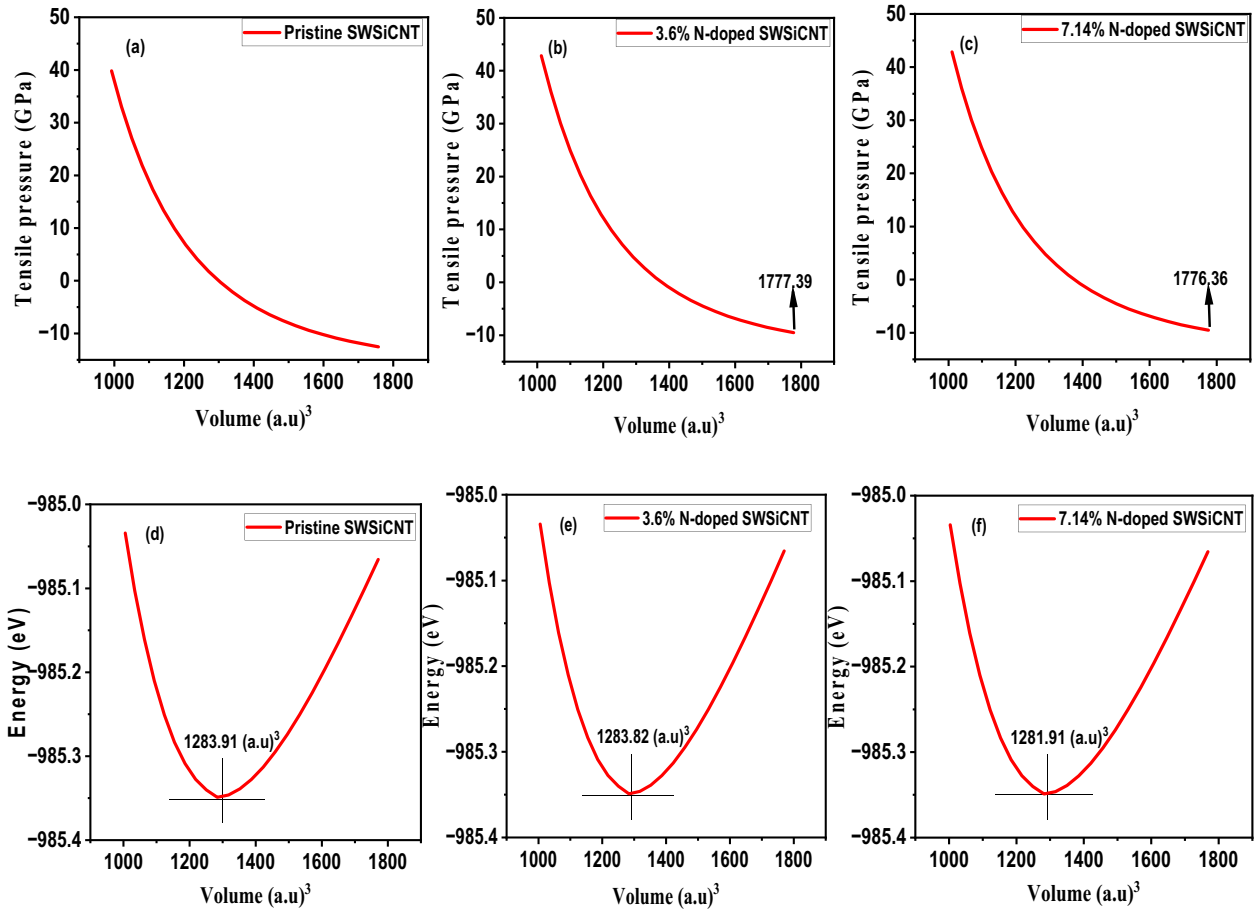

Figure 3. Effects of tensile pressure on the volume of (a) pristine SWSiCNT (b) 3.6%N-doped SWSiCNT (c) 7.4% N-doped SWSiCNT, and effects of total energy on the volume of (d) pristine SWSiCNT (e) 3.6% N-doped SWSiCNT and (f) 7.4% N-doped SWSiCNT.

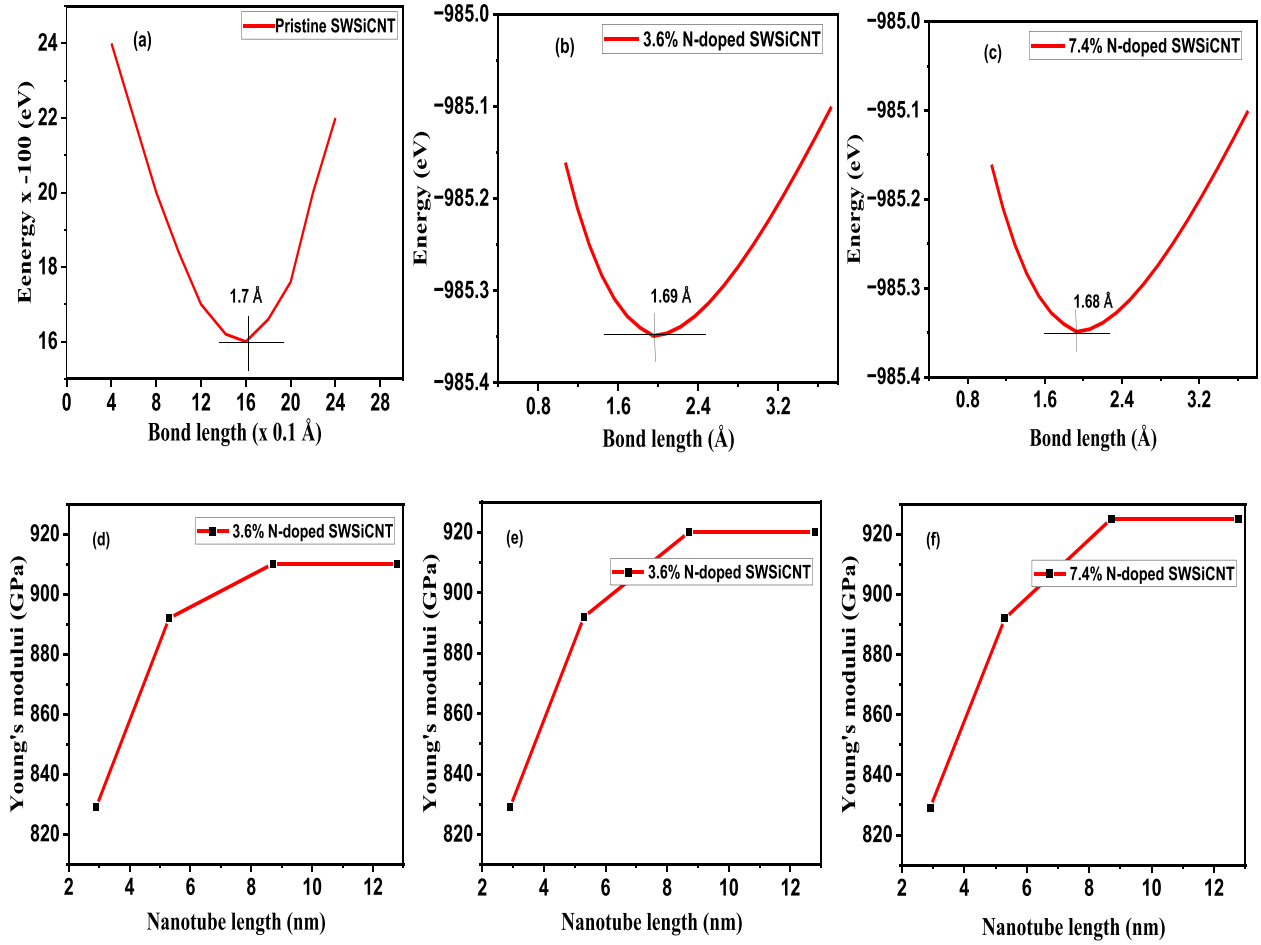

Figure 4. Effects of bond energies on bond lengths of (a) pristine SWSiCNT (b) 3.6% N-doped SWSiCNT, (c) 7.4% N-doped SWSiCNT. The calculated Young's moduli for (d) pristine SWSiCNT, (e) 3.6% N-doped SWSiCNT and (f) 7.4% N-doped SWSiCNT.

Table 2. Calculated elastic parameters of the investigated systems.

Material	Bond length (Å)	Bond energy (eV)	Volume (a.u)^3	Stress (GPa)	Young's Modulus (GPa)
Pristine (7, 7) SWSiCNT	1.71	−985.35	1283.91	11.12	910.35
3.6% N-doped SWSiCNT	1.69	−985.34	1283.82	10.92	920.86
7.4% N-doped SWSiCNT	1.68	−985.30	1282.91	10.51	923.41

them stronger and therefore able to withstand unfavorable changes in mechanical states. To confirm this statement, we found that the calculated bond lengths of all three systems were inversely proportional to the bond order. Strong bond orders are therefore accompanied by strong attractive forces that hold the interacting atoms together. Furthermore, for all three systems, the inverse variations in bond energy with bond length were due to repulsive forces, while the obtained direct variations in bond energies were due to attractive forces. On this basis, it was found that the stability of the N-doped systems shows a significant increase, thus requiring higher enthalpy to break the bond. Figure 4(d–f) show the analysis of the calculated Young's moduli of the investigated systems with different lengths of the nanotubes. The 7.4% N-doped SWSiCNT was found to be stiffer due to the reduced bond length and higher dopant concentration, while pure SWSiCNT exhibited lower stiffness due to longer bond length. A summary of the calculated mechanical properties of the original SWSiCNT, 3.6% N-doped, and 7.4% N-doped SWSiCNT structures is presented in Table 2. It can be seen from the Table that this doping does not cause any significant change in the structural properties of the systems studied. For example, the volume of the original SWSiCNT changed by only 0.09 (a.u)^3 when 4.6% N atom was doped and by 1 (a.u)^3 when 7.4% N atom was doped. Therefore, it can be concluded that our doped SWSiCNT system is structurally and mechanically stable for further investigation of its photocatalytic properties.

3.2 Electronic properties

To obtain relevant data on the electronic properties of the N-doped (7, 7) SWSiCNT photocatalyst, it is crucial to understand its pristine electronic behavior. For this reason, we first analyzed the electronic properties of the pure (7, 7) SWSiCNT system. The results are shown in Figure 5(a) and the calculations were

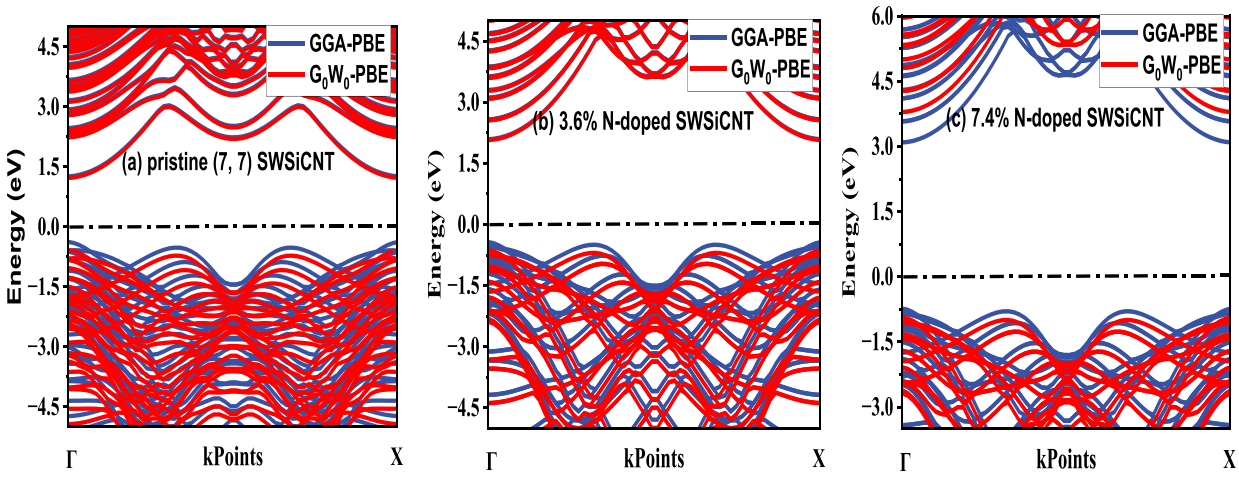

Figure 5. Electronic band gaps of (a) pristine SWSiCNT (b) 3.6% N-doped SWSiCNT and (c) 7.4% N-doped SWSiCNT.

performed with both Kohn-Sham DFT and GW approximations (GWA). Results from KS-DFT using the GGA-PBE exchange function revealed a bandgap of 1.6 eV. In addition, it can be seen that both the valence band and the conduction band have the same momentum. For this reason, the obtained band gap of the pristine SWSiCNT is a direct band gap and this agreed well with the obtained experimental values [37]. Therefore, this type of material generates light during the recombination of electrons and holes (high charge carrier concentration). Due to the reported bandgap problem by the GGA functional, we have repeated our calculations using the hybrid GW within the G_0W_0 approximation and obtained accurate results in which a band gap of 1.7 eV was obtained. Also, the VBM was found to be −0.3 eV which is less than the normal value of −0.77 eV for OER. Similarly, the CBM was found to be 1.2 eV which is also less than 1.23 eV for HER. Therefore, pristine SWSiCNT does not satisfy the condition to serve as a photocatalyst for water splitting because the band gap value of 1.7 eV is outside the range of 2.3 eV to 2.8 eV for efficient absorption of visible light. To tune the pure (7, 7) SWSiCNT, we doped the system with 3.6% nitrogen and observed changes in its electronic behavior after doping. Later on, we increased the N-dopant concentration to 7.4% and different behaviors were observed. Figure 5(b) shows the results of the calculated electronic band gap of the 3.6% N-doped SWSiCNT system. The effect of the N-doping can be seen through the shift of the bands from 1.7 eV to 2.54 eV (with KS-DFT) and 2.56 eV (with G_0W_0) which is blue-shifted. It is shown that both KS-DFT and GW methods report a band gap within a specified range for photocatalysts. The obtained band gap (2.56 eV) of the 3.6% N-doped SWSiCNT was found to be greater than the reported 1.23 eV for hydrogen evolution [38] by water splitting, and this presents overpotential to overcome the energy variation of the SWSiCNT photocatalyst. It also falls within the range of 2.2 eV to 2.8 eV. Additionally, N-doping promoted a decrease in charge carrier concentration which also reduces electron–hole recombination. As a result, the electronic motion becomes limited and trapped by N-impurities. Therefore, hydrogen reduction can take place by the photo-generated electrons of the 3.6% N-doped SWSiCNT. Moreover, the potential of the VBM was found to be −0.4 eV which is lower than −0.77 eV for normal OER [39]. The CBM was also analyzed and found to be 2.1 eV which is also greater than HER [40] potential of 0.02 eV [23], thus indicating that hydrogen can be liberated well on the active sites of N-doped SWSiCNT (3.6%). Based on this, the 3.6% N-doped SWSiCNT demonstrated itself as a better photocatalyst for hydrogen evolution via the water-splitting process.

The widening of the band gap of the N-doped SWSiCNT is due to the atomic orbitals of hydrogen atoms transforming into a series of energy levels as a result of quantum mechanical occupations of the equilibrium band by many electrons. It is also due to interactions between lattice phonons of the pure SWSiCNT and free holes of N atoms as a result of increased charge carrier concentration [41]. Furthermore, the carrier concentration and electrical conductivity of SiCNT decrease with pentavalent nitrogen atoms due to the intra-atomic cluster [42]. As presented in Figure 5(c), an increase in the concentration of N atoms further broadened the band gap to the tune of 4.3 eV which is outside the standard range for photocatalysts to have perfect interactions with photons in the visible region. Therefore, it can be reported that the N-doped SWSiCNT photocatalyst performs better when 3.5% of N-dopant is used to dope one unit cell of the nanotube. Based on this, we can report that N-doped SWSiCNT can be a better water-splitting photocatalyst when the minimum energy state in the conduction band occurs at the

conduction band edge of 2.1 eV and the maximum energy state in the balance band occurs at the band edge of 0.4 eV.

Analysis of the variation of the dopant concentration with the calculated band gaps of the SWSiCNT system was performed appropriately, and obtained results are presented in Figure 6(a,b). As shown in Figure 6(a), both GGA and G_0W_0 results reveal that the band gap of pristine SWSiCNT broadens as the N-concentration increases. Compared with Figure 6(b), it can be seen that one atom of Nitrogen corresponds to 3.6%, while two atoms of nitrogen correspond to 7.4%. Therefore, to achieve optimum performance by SWSiCNT photocatalyst, the sample shall be prepared such that one N atom per unit cell of SWSiCNT is obtained.

In order to know the degree of occupation and the density of electrons in a given state, it is necessary to obtain a detailed description of its electronic density of states (DOS), which is possible by analyzing the number of different energy states at a given energy level. Figure 7(a–c) show the overall density of states for both pristine and N-doped SWSiCNT structures under different concentrations. Although both systems registered empty states at the Fermi level, the probability of finding electrons at the Fermi level is higher for the pristine SWSiCNT than for the N-doped SWSiCNT. Therefore, the band gaps in the doped systems are wider. In addition, a higher intensity of the DOS in Figure 7(b) indicates that the energy populations in the doped system are higher than in the pristine system. In addition, the shapes of the DOS patterns are almost similar except in the area corresponding to 5 eV in Figure 7(b), which has a lower intensity than the same 5 eV area in Figure 7(a). Because at this point in the conduction band, N atoms took up space for themselves. Therefore, the band gap opening in the doped system was due to the effects of N atoms in the conduction band. To obtain different orbital contributions to the photocatalytic potentials of the N-doped SWSiCNT, PDOS calculations were performed and the results are shown in Figure 8. Although N orbitals show the highest valence band occupation, there is no contribution between

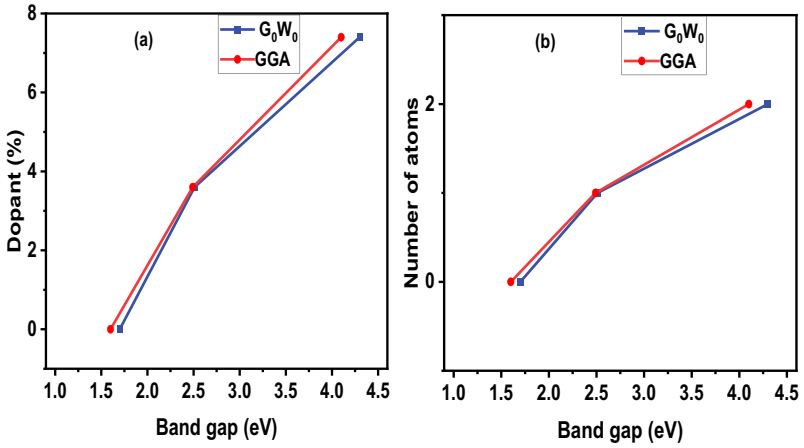

Figure 6. (a) Variation of N concentration with a band gap of SWSiCNT (b) variation of number of N atoms with a band gap of SWSiCNT.

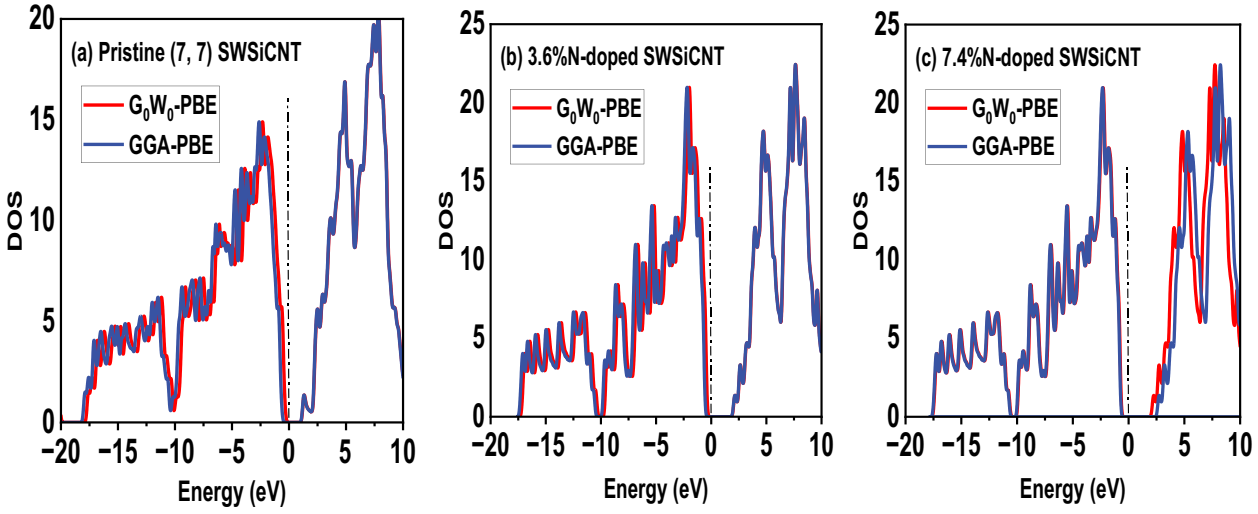

Figure 7. DOS of (a) Pristine SWSiCNT (b) SWSiCNT doped with 3.6%wt N (c) SWSiCNT doped with 7.4%wt N.

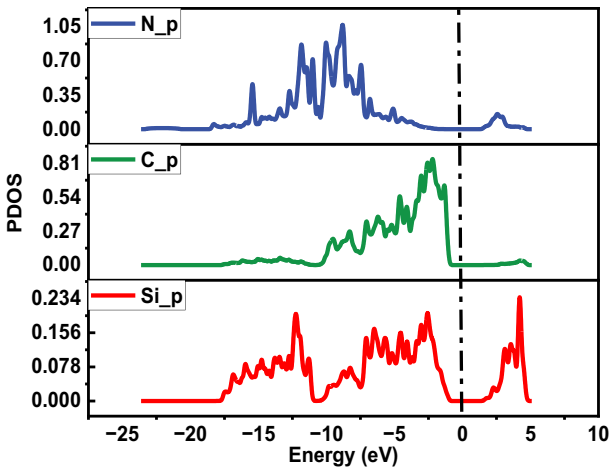

Figure 8. PDOS of the 3.6% N-doped SWSiCNT photocatalyst.

valence band maxima (VBM) and conduction band minima (CBM). C orbital behavior was observed very close to the Fermi level near the VBM and showed no contribution in the conduction band. Regarding Si orbitals, clear features were observed in both VBM and CBM. Therefore, the widening of the band gap of the N-doped SWSiCNT is due to the blue shift by Si orbitals as a result of the occupation of spaces in the conduction band by N orbitals.

To further analyze the electronic behaviors of the investigated systems, we report the effects of tensile pressure (stress) and Young's modulus on the band gaps of the SiC nanotube systems. The results of the analysis are presented in Figure 9(a,b). It has been observed that the band gap of the SWSiCNT photocatalyst was found to decrease from 4.3 eV (3.35 eV with GGA) to 1.25 eV (1.1 with GGA) with external pressure from 10.51 GPa to 11.12 GPa because when external pressure is increased, gamma states are produced in the energy band gap [43]. Figure 9(b) also reveals that Young's modulus increases with decreasing band gap, which agrees well with the reported mechanical behaviors of carbon nanotubes photocatalysts [44]. Therefore, the nanotube structure doped with 7.4% N atoms demonstrated higher mechanical strength, while pristine SWSiCNT showed the lowest mechanical strength.

3.3 Optical properties

Analysis of an optoelectronic system cannot be completed until there is an adequate description of its behavior related to the interactions with electromagnetic waves. For an electronic system, the optical response to the incident electromagnetic waves is determined from the real and imaginary dielectric functions given by [45], as expressed by Equation (6),

$$\varepsilon(\omega) = \varepsilon_1(\omega) + \varepsilon_2(\omega) \tag{6}$$

Where $\varepsilon_1(\omega)$ is the real part and $\varepsilon_2(\omega)$ is the imaginary part of the optical dielectric constant. The real part of the dielectric function describes the photon dispersion, while the imaginary part of the dielectric function describes the photon absorption. In the present study, we consider the imaginary part of the dielectric function to analyze the amount of solar energy absorbed by the pristine and doped SWSiCNT structures under different nitrogen dopant concentrations. For these studies, the optical absorption spectra were examined in both parallel and perpendicular directions. Furthermore, the studies were conducted using the random-phase approximation method which takes care of the electron–electron interactions only. Figure 10(a) shows the optical absorption spectra of the pristine SWSiCNT with respect to the imaginary dielectric function. As can be seen, pristine SWSiCNT shows higher energy absorption in directions parallel than perpendicular to the nanotube axis. Few absorption peaks also appeared at 1.3 eV and 2.1 eV in the perpendicular direction. Based on the different behaviors observed by nanotubes in different directions, it can be called anisotropic. High intensities were recorded at 5.1 eV in both directions, corresponding to the ultraviolet range. 5.1 eV is also higher than the experimental optical gap of efficient

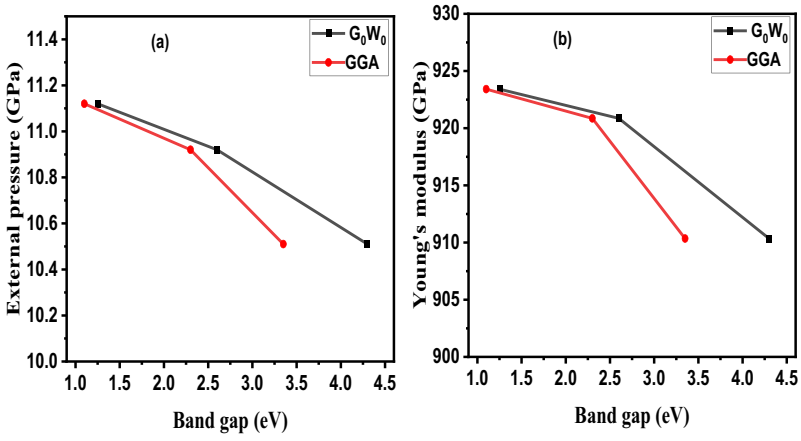

Figure 9. Band gap variation with (a) tensile pressure and (b) Young's modulus of SWSiCNT photocatalyst under N doping.

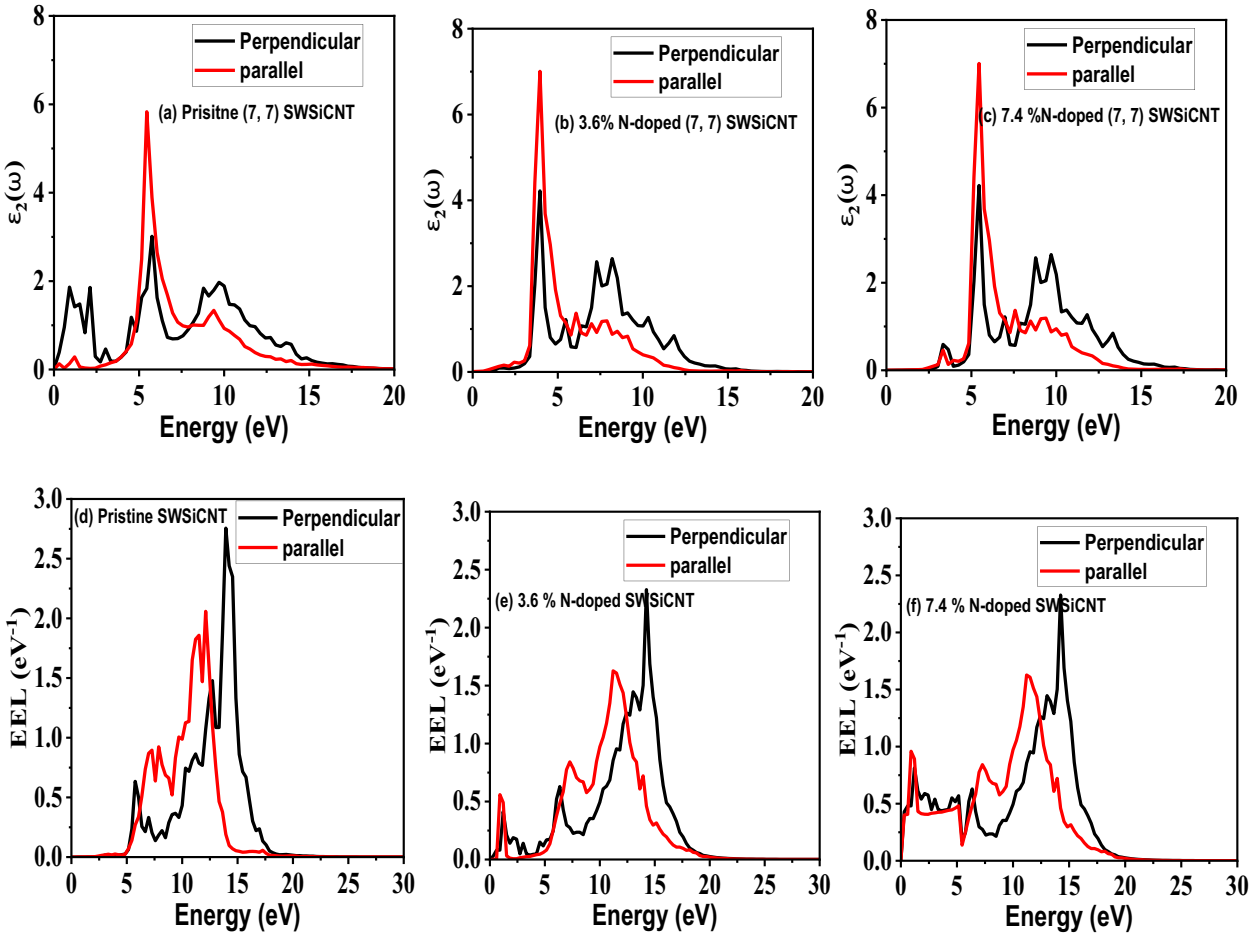

Figure 10. Photon absorption by (a) pristine SWSiCNT, (b) 3.6% N-doped SWSiCNT and (c) 7.4% N-doped SWSiCNT photo-systems. Electron energy loss spectra of (d) pristine SWSiCNT (e) 3.6% N-doped SWSiCNT and (f) 7.4% N-doped SWSiCNT.

photocatalysts, hence the pure (7, 7) SWSiCNT is considered an unsuitable photocatalyst. The N-doped SWSiCNT photocatalyst shown in Figure 10(b) shows good performance, consistent with other perfect photocatalysts [46,47]. It absorbs a high amount of energy at a band edge of 2.7 eV, which is in the visible range. In addition, its absorption is both parallel and perpendicularly symmetric, with a high absorption being recorded in parallel. Absorption at 2.7 eV means that the doped SWSiCNT interacts with visible electromagnetic energy from 2.2 eV to 2.8 eV range for photocatalysis. Therefore, the optimized system of N-doped (7, 7) SWSiCNT can be considered a better photocatalyst for the whole water-splitting technology. Figure 10(c) reveals different behaviors of the N-doped SWSiCNT system when the percentage doping was increased to 7.4%. A new and smaller peak can be seen at 3.89 eV as a result of increased doping. The material also absorbs a higher number of photons in the ultraviolet region, which accounts for only 3% of solar radiation. Therefore, the 7.4% N-doped SWSiCNT is regarded as an unsuitable photocatalyst but can be used for other applications such as medical treatments using UV light. The energy loss function analysis was performed on all systems examined. Figure 10(d) shows that pristine SWSiCNT neither emits nor absorbs photons below 5 eV. More energy losses were also recorded in the UV range. Relative to 3.6% N-doped SWSiCNT, there were significantly lower electron energy losses in the range corresponding to 2.7 eV, which corresponds to the obtained optical band gap of this photocatalyst. This behavior indicates that higher photon energy is absorbed in this region, which agrees well with the absorption spectra previously reported in Figure 10(b). Figure 10(f) shows higher energy loss than 3.6% SWSiCNT, which means it showed poor absorption in the visible range.

A summary of the obtained characteristics of the investigated systems can be found in Table 3. As can be seen, the N-doped SWSiCNT photocatalyst performs efficiently when 3.6% of N dopant is used per unit cell of the pristine SWSiCNT because the N atoms have strong coulombic interactions with Si and C atoms [48]. At this concentration, more photon energies were absorbed, interactions took place in the visible range and both electronic and optical band gaps correlated very well with the obtained theoretical data. Analysis of the absorption

Table 3. Summary of the obtained characteristics of the investigated systems.

Material	The electronic band gap (eV)	The optical band gap (eV)	Dielectric absorption (a.u)	Remark
Pristine SWSiCNT	1.7	1.6	6.10	Unsuitable
3.6% N-doped SWSiCNT	2.56	2.70	7.42	Suitable
7.4% SWSiCNT	4.30	4.81	7.32	Unsuitable

Table 4. Effects of absorption and binding energies.

Absorbing surface	Bond angle (degrees)	Bond length (nm)	Absorption energy (eV)	Binding energy (Ve)	Reference
Pristine SWSiCNT	102.02	1.71	−1.81	−11.55	[49]
3.6% N-doped SWSiNT	102.21	1.69	−1.97	−11.48	[50]
7.4% N-doped SWSiNT	101.91	1.68	−1.91	−11.53	[51]

Table 5. Previous work vs current work.

Material	Method	ε_2 (a.u)	The band gap (eV)
N-doped TiO_2 nanotubes [52]	Experimental hydro-thermal process	19.11	2.7
C-doped TiO_2	Experimental synthesis method	18.52	2.4
BN-CNT heterostructure [53]	DFT- first principles	Not reported	2.51
Co-doped CNTs [54]	DFT-first principles	23.20	2.55
3.6% N-doped SWSiCNT- current work	DFT with absorption optical spectra analysis	21.53	2.56

energy presented in Table 4 also reveals that 3.6% N-doped SWSiCNT absorbs more energy than the pristine and 7.4% N-doped SWSiCNT systems. This table also shows that atoms in pristine SWSiCNT are more bound together than in the doped systems. Table 5 presents various reports from some available literature regarding materials' photoactivity in the water-slitting process. It has been found that C-doped TiO_2 photocatalyst [55] and the results from current work present a very good photocatalytic performance. Additionally, the optical and electronic band gaps of these materials are in good agreement with each other. Therefore, the ability of the Si-doped SWZnONT can be enhanced by the photo-generated holes in the Si-doped ZnO nanotube surface. Based on this, hydrogen can be

Table 6. A critical comparison between some selected past works and the current work.

Materials	Analysis	Application	Reference
SWSiCNT	Zheng et al. only report the field emission potentials of the SWSiCNT without considering chirality. While the present work investigated the N-doped system of SWSiCNT with (7, 7) chirality for the production of hydrogen.	Does not specifically state the most suitable area of application of the investigated nanotubes while current work found the material worthy of use as a photocatalyst.	[56]
N-doped (6, 0) and (4, 4) SWSiCNT	Results demonstrated that N impurities do not alter the structure of SWSiCNT which agreed well with the current work. Our findings also revealed that the characteristic surface reactivity of the (7, 7) SWSiCNT was generally influenced by doping of 3.6% nitrogen. However, our work is different because we have extended the studies to the mechanical and optical characteristics of the (7, 7) SWSiCNT.	Mahdaviani et al. investigated the surface reactivity of the N-doped SWSiCNT while the current work studied the photocatalytic potentials of N-doped SWSiCNT	[57]
SWSiCNT doped with B, N and O at once	Maghnaoui and Boufelfel studied the effect of magnetic moment on the doped SWSiCNT without a complete description of the electronic and optical properties. While the current work investigated the effects of different nitrogen concentrations on the doped SWSiCNT which was found to make a significant effect on the electronic and optical properties of the nanotube.	Maghnaoui and Boufelfel did not specify possible areas of applications of their obtained results. The current work recommended the N-doped SWSiCNT as good photocatalysts for hydrogen production.	[58]
Metal decorated SiCNT	Results revealed that metal-decorated SiCNT can actively adsorb hydrogen in the visible region. In the current work, a non-metal doped (N-doped) SWSiCNT was found to absorb solar energy very well in the visible range.	Ram et al. recommended metal-doped SiCNT as a good candidate for hydrogen storage while the current work found N-doped (non-metal) SWSiCNT as a good candidate for hydrogen production.	[59]
Hydrogen boride nanotubes with C, N and O decoration	Results by Nontawat et al. showed that N-doped hydrogen boride could be used to store hydrogen. However, the scope of our work is entirely on a different material and for hydrogen production not for hydrogen storage.	Doped hydrogen boride by Nontawat et al. was found worthy for water-sensing applications while the current work found N-doped SiCNT for water-splitting applications.	[60,63]
Metal decorated SiCNTs	Results by Singh revealed that CO_2 adsorption on Cu-decorated SiCNT undergoes spontaneous exothermic reaction.	Singh reported the possible potential of metal-decorated SiCNT for CO_2 storage. Their work, however, found the material unsuitable for such application. In our work, we studied non-metal doped SiCNT as a catalyst for producing hydrogen only and it was found worthy applicable.	[61,62]

produced when protons produced by water splitting penetrate the Si atom and react with the photo-generated electrons on the ZnO nanotube [64,65].

In terms of potential application areas, Table 6 presents the data obtained from the previous work in comparison with the current work. As shown, several works were performed on either the pristine SiCNT or the doped systems of SiCNTs. However, its potential to serve as a photocatalyst to produce hydrogen under solar irradiation has not been explored except in the current work. Therefore, the novelty of this work offers more possibilities to use the versatile properties of these nanotubes for a wide range of applications.

4. Conclusions

This study reports the photocatalytic properties of the nitrogen-doped single-walled silicon carbide nanotube based on the analysis of structural, elastic, electronic and optical features of this semiconductor. All calculations for the aforementioned properties of the investigated systems were done using the popular density functional theory as implemented in quantum ESPRESSO and Yambo codes. Doping of the pristine SWSiCNT system was performed using different concentrations of nitrogen atoms. It has been observed that the diameter of the SWSiCNT decreased from 30.01 Å to 29.51 Å and 29.02 Å when 3.6 wt% and 7.4 wt% N dopants were used. Additionally, it was found that the electronic band gap varies directly with N concentration and inversely with tensile pressure and Young's modulus. A better photocatalytic performance (energy range of 2.2 eV−2.8 eV) was found with the 3.6% N-doped SWSICNT which demonstrated electronic and optical band gaps of 2.56 eV and 2.70 eV, respectively. Finally, the observed structural, mechanical, electronic and optical behaviors demonstrated by the N-doped SWSiCNT expose it as a better photocatalyst for hydrogen production under the visible light/energy spectrum. On the final note, it is recommended that these materials should be synthesised and analysed in order to identify any potential differences between experimental and theoretical data.

Acknowledgments

The authors acknowledged the contribution of the Tertiary Education Trust Fund (TETFund) for funding and Bauchi State University, Gadau in all aspects to the successful completion of this research.

Disclosure statement

No potential conflict of interest was reported by the author(s).

Funding

The authors extend their appreciation to the Deanship of Scientific Research at King Khalid University for funding this work through a large group research project under grant number (R.G.P.2/324/44).

ORCID

Abubakr M. Idris http://orcid.org/0000-0003-4038-4769
Mayeen Uddin Khandaker http://orcid.org/0000-0003-3772-294X

Author contributions

Conceptualization, Y.S.I. and M.U.K.; methodology, Y.S.I. and R.R.; software, Y.S.I., R.R., H.O., M.K. and S.T.; formal analysis, Y.S.I., R.R., and S.T.; resources, R.R., H.O., M.K. and A.M.I.; data curation, M.U.K. and Y.S.I.; writing – original draft preparation, Y.S.I.; writing – review and editing, M.U.K.; visualization, M.U.K., S.T., H.O., M.K. and A.M.I. All authors have read and agreed to the published version of the manuscript.

Data availability statement

All data that we used in this manuscript regarding quasi-particle energies, band structure, DOS and optical spectra analysis were analysed and obtained with the quantum ESPRSSO codes, which are freely available at www.quantumespresso.org. Corrections to quasi-particle interactions are done via Yambo interacting codes at www.yambo.org. We have optimized the geometric system of gallium nitride nanotubes by using 'tubegen' database which is freely available at https://turin.nss.udel.edu/research/tubegenonline.html.

Ethics

Procedures for data collection and study protocols were permitted by Bauchi State University's Centre for Excellence in Research and Innovation, and were conducted according to the guidelines declared. Also, no human parts were used in the conduct of this research.

References

[1] Itas YS, Khandaker MU, Abdussalam BS, et al. Studies of H2 storage efficiency of metal-doped carbon nanotubes by optical adsorption spectra analysis. Diam Relat Mater. 2023;136:109964.
[2] Fang W, Jean DH, Zhizhang Y, et al. Technologies and perspectives for achieving carbon neutrality. Innovation. 2021;2:100180.
[3] Curco D, Gimenez J, Addardak A, et al. Effects of radiation absorption and catalyst concentration on the photocatalytic degradation of pollutants. Catal Today. 2002;76(2–4):177–188. doi: 10.1016/S0920-5861(02)00217-1
[4] Ziyang Z, Lei B, Hao T, et al. Tailoring the surface and interface structures of copper-based catalysts for electrochemical reduction of CO2 to ethylene and

ethanol. Small. 2022;18:2107450. doi: 10.1002/smll.202107450
[5] Zi-Yang Z, Hao T, Lei B, et al. Cu-Zn-based alloy/oxide interfaces for enhanced electroreduction of CO2 to C2+ products. J Energy Chem. 2023;83:90–97. doi: 10.1016/j.jechem.2023.04.034
[6] Min L, Jietian Y, Xingang L, et al. Insights into alloy/oxide or hydroxide interfaces in Ni–Mo-based electrocatalysts for hydrogen evolution under alkaline conditions. Chem Sci. 2023;14:3400–3414. doi: 10.1039/D2SC06298D
[7] Hyemin K, Jeonggyun H, Honghyun C. Evaluation of solar energy absorption and photo-thermal conversion performance of SiC/ITO hybrid nanofluid. Case Stud Thermal Eng. 2022;35:102151. doi: 10.1016/j.csite.2022.102151
[8] Yahaya IS, Razali R, Tata S, et al. Studies of the hydrogen energy storage potentials of Fe- and Al-doped silicon carbide nanotubes (SiCnts) by optical adsorption spectra analysis. J Energy Storage. 2023;72:108534. doi: 10.1016/j.est.2023.108534
[9] Jiang Z, Xiao T, Kuznetsov VL, et al. Turning carbon dioxide into fuel. Math Phys Eng Sci. 2010;368:0119. doi: 10.1098/rsta.2010.0119
[10] Yadala VD, Nagappagari LR, Kiyoung L, et al. Optimization of N doping in TiO2 nanotubes for the enhanced solar light mediated photocatalytic H2 production and dye degradation. Environ Pollut. 2021;269:116170. doi: 10.1016/j.envpol.2020.116170
[11] Yahaya SI, Abdussalam BS, Chifu EN, et al. Effects of SiO2 and CO2 absorptions on the structural, electronic and optical properties of (6, 6) magnesium oxide nanotube (MgONT) for optoelectronics applications. Silicon. 2023;2023:1–12.
[12] Babayan M, Mazraeh AE, Yari M, et al. Hydrogen production with a photovoltaic thermal system enhanced by phase change materials, shiraz, Iran case study. J Clean Prod. 2019;215:1262–1278. doi: 10.1016/j.jclepro.2019.01.022
[13] Yahaya IS, Isah KA, Nuhu AH, et al. The potentials of boron-doped (nitrogen deficient) and nitrogen-doped (boron deficient) BNNT photocatalysts for decontamination of pollutants from water bodies. RSC Adv. 2023;13:23659–23668.
[14] Yuan L, Fei X, Wenhao L, et al. MoS2 with structure tuned photocatalytic ability for degradation of methylene blue. IOP Conf Ser. 2019;300:052021. doi: 10.1088/1755-1315/300/5/052021
[15] Haodong J, Jinren N, Dongye Z, et al. Application of titanate nanotubes for photocatalytic decontamination in water: challenges and prospects. ACS EST Eng. 2022;2(6):1015–1038. doi: 10.1021/acsestengg.1c00451
[16] Fabiola M, Santiago E, Jaime G. Photocatalytic degradation of non-steroidal anti-inflammatory drugs with TiO2 and simulated solar radiation. Water Res. 2008;42:585–594. doi: 10.1016/j.watres.2007.08.002
[17] Jingwen W, Yusuke A, Shu Y. Preparation of (Zn1+xGe)(N2Ox) nanoparticles with enhanced NOx decomposition activity under visible light irradiation by nitridation of Zn2GeO4 nanoparticles designed precisely. Nanoscale. 2019;11:20151–20160.
[18] Yusuke A, Yoshiyuki I, Koichiro U, et al. Synthesis of gallium oxynitride nanoparticles through hydrothermal reaction in the presence of acetylene black and their photocatalytic NOx decomposition†. Nanoscale. 2018;10:1837–1844. doi: 10.1039/C7NR07502B
[19] Jingwen W, Yusuke A, Takuya H, et al. High-concentration N-doped La2Ti2O7 nanocrystals: effects of nano-structuration and doping sites on enhancing the photocatalytic activity. Chem Eng J. 2021;423:130220. doi: 10.1016/j.cej.2021.130220
[20] Itas YS, Abdussalam BS, Chifu EN, et al. First-principle studies of the structural, electronic, and optical properties of double-walled carbon boron nitride nanostructures heterosystem under various interwall distances. J Chem. 2023;2023:4574604. doi: 10.1155/2023/4574604
[21] Hamidreza J, Hossein F, Mohamad MM. A DFT study of the water-splitting photocatalytic properties of pristine, Nb-doped, and V-doped Ta3N5 monolayer nanosheets. Surf Interfaces. 2021;26:101379. doi: 10.1016/j.surfin.2021.101379
[22] Hefeng Z, Jiaqi L, Ting X, et al. Recent advances on small band gap semiconductor materials (≤2.1 eV) for solar water splitting. Catalysts. 2023;13:728.
[23] Quan L, Zhen F, Wang D. Theoretical study on the electrochemical water splitting of two-dimensional metal-organic frameworks TM3C12O12 (TM = Mn, Fe, Co, Ni). Crystals. 2022;12:1289.
[24] Aminu YS, Shaari A, Isah I, et al. Effects of exchange correlation functional (Vwdf3) on the structural, elastic, and electronic properties of transition metal dichalogenides. J Niger Soc Phys Sci. 2023;5:1094.
[25] Yahaya SI, Abdussalam BS, Chifu EN, et al. DFT studies of structural, electronic and optical properties of (5, 5) armchair magnesium oxide nanotubes (MgOnts). Physica E Low Dimens Syst Nanostruct. 2023;149:115657.
[26] Yahaya IS, Suleiman AB, Ndikilar CE, et al. Effects of oxygen absorption on the electronic and optical properties of armchair and zigzag silicon carbide nanotubes (SiCnts). Phys Scr. 98(1):2023. doi: 10.1088/1402-4896/aca5cf
[27] Yahaya SI, Razif R, Salisu T, et al. DFT studies on the effects of C vacancy on the CO2 capture mechanism of silicon carbide nanotubes photocatalyst (Si12C12-X; X = 1; 2). Silicon. 2023;2023:1–11.
[28] Oberhofer H. Electrocatalysis beyond the Computational hydrogen electrode. In: Andreoni W, editor. Handbook of materials modeling. Cham: Springer; 2018. p. 1–33.
[29] Shehu AY, Amiruddin S. First-principles study on the structural, electronic, and elastic properties of transition metal dichalcogenides. Phys Access. 2023;3:133.
[30] Yahaya SI, Abdussalam BS, Chifu EN, et al. Computational studies of the excitonic and optical properties of armchair SWCNT and SWBNNT for optoelectronics applications. Crystals. 2022;12:870. doi: 10.3390/cryst12060870
[31] Itas YS, Baballe A, Danmadami MD, et al. Analysis of different welding speeds and the micro structure on the welded joints of silicon steel pipe. IOP Conf Ser. 2020;932:012123.
[32] Yiyu F, Xianggang K, You Y, et al. First-principles study of the effect of dopants (Pd, Ni) on the formation and desorption of T2O from a Li2TiO3 (001) surface. RSC Adv. 2019;9:8490–8497.
[33] Cristiano C, Viviana S, Ruggero A, et al. Effect of nitrogen and aluminum doping on 3C-SiC

heteroepitaxial layers grown on 4° Off-axis Si (100). Mater (Basel). 2021;14:4400.
[34] Cho J, Joshi MS, Sun CT. Effect of inclusion size on mechanical properties of polymeric composites with micro and nano particles. Compos Sci Technol. 2006;66(13):1941–1952. doi: 10.1016/j.compscitech.2005.12.028
[35] Tasiu Z, Yahaya SI, Chifu EN. Carbon nanotubes: a review of Synthesis and characterization methods/techniques. Int J Sci Tech. 2020;8:43–50. doi: 10.24940/theijst/2020/v8/i2/ST2002-020
[36] Susi T, Skakalova V. Computational insights and the observation of SiC nanograin assembly: towards 2D silicon carbide. Sci Rep. 2017;7:4399.
[37] Itas YS, Abdussalam BS, Chifu EN, et al. The exchange-correlation effects on the electronic bands of hybrid armchair single-walled carbon boron nitride nanostructure. Crystals. 2022;12:394. doi: 10.3390/cryst12030394
[38] Waterhouse GI, Wahab AK, Al-Oufi M, et al. Hydrogen production by tuning the photonic band gap with the electronic band gap of TiO2. Sci Rep. 2013;3:2849. doi: 10.1038/srep02849
[39] Ravi K, Xi C, Xueqing Z, et al. Electrochemical water oxidation on WO3 surfaces: a density functional theory study. Catal Today. 2019;321:94–99. doi: 10.1016/j.cattod.2018.02.030
[40] Wenyi T, Guangzhao W, Can F, et al. Engineering two-dimensional SnC/HfSSe heterojunction as a direct Z-scheme photocatalyst for water splitting hydrogen evolution. Appl Surface Sci. 2023;626:157247. doi: 10.1016/j.apsusc.2023.157247
[41] Vladimir A, Burdov A, Mikhail I. Exciton-photon interactions in semiconductor nanocrystals: radiative transitions, non-radiative processes and environment effects. Appl Sci. 2021;11:497. doi: 10.3390/app11020497
[42] Shamsa M, Syed Mujtaba S, Hazrat H, et al. Effect of carrier concentration on the optical band gap of TiO2 nanoparticles. Mater Design. 2016;92:64–72. doi: 10.1016/j.matdes.2015.12.022
[43] Itas YS, Chifu EN, Khandaker MU. Synthesis of thermally stable h-BN-CNT hetero-structures via microwave heating of ethylene under nickel, iron, and silver catalysts. Crystals. 2021;11:1097. doi: 10.3390/cryst11091097
[44] Zhang T, Latha K, Du GH, et al. Mechanical properties of carbon nanotube–alumina nanocomposites synthesized by chemical vapor deposition and spark plasma sintering. Compos Part A Appl Sci Manuf. 2009;40:86–93. doi: 10.1016/j.compositesa.2008.10.003
[45] Yahaya IS, Suleiman AB, Ndikilar CE, et al. DFT studies of the photocatalytic properties of MoS2-doped boron nitride nanotubes for hydrogen production. ACS Omega. doi: 10.1021/acsomega.3c05907
[46] Bayarri B, Gimenez J, Curco D, et al. Photocatalytic degradation of 2, 4-dichlorophenol by TiO2/UV: kinetics actinometries and models. Catalyst Today. 2005;101:227–236. doi: 10.1016/j.cattod.2005.03.019
[47] Ameena N, Khan MI, Naeem MA, et al. Structural, morphological, optical, and photocatalytic properties of Ag-doped MoS2 nanoparticles. J Mol Struct. 2020;1220:128735. doi: 10.1016/j.molstruc.2020.128735
[48] Chen N, Can F, Biao W, et al. Charge-compensated codoped pseudohexagonal zinc selenide nanosheets towards enhanced visible-light-driven photocatalytic water splitting for hydrogen production. Int J Hydrogen Energy. 2021;46:34305–34317. doi: 10.1016/j.ijhydene.2021.08.023
[49] Ram SS, Ankit S. Modulation of electronic properties of silicon carbide nanotubes via sulphur-doping: an ab initio study. Phys Lett A. 2016;380:1201–1204. doi: 10.1016/j.physleta.2016.01.029
[50] Jing-Xiang Z, Yi-Hong D. Silicon carbide nanotubes functionalized by transition metal atoms: a density-functional study. J Phys Chem C. 2008;112:2558–2564. doi: 10.1021/jp073722m
[51] Lin Z, Zhen C. First-principles study of metal impurities in silicon carbide: structural, magnetic, and electronic properties. Front Mater. 2022;9:956675. doi: 10.3389/fmats.2022.956675
[52] Yadala VD, Nagappagari LR, Kiyoung L, et al. Optimization of N doping in TiO2 nanotubes for the enhanced solar light mediated photocatalytic H2 production and dye degradation. Environ Pollut. 2021;269:116170. doi: 10.1016/j.envpol.2020.116170
[53] Xiaohan S, Hongxia B, Yingcai F, et al. Photocatalytic hydrogen production and storage in carbon nanotubes: a first-principles study. RSC Adv. 2022;12:17029–17035. doi: 10.1039/D2RA02349K
[54] Lianming Z, Sheng G, Liu H, et al. Density functional study of hydrogen evolution on cobalt-embedded carbon nanotubes: effects of doping and surface curvature. ACS Appl Nano Mater. 2018;1:6258–6268. doi: 10.1021/acsanm.8b01466
[55] la Cruz N D, Dantas NR, Geimenez R, et al. Photolysis and TiO2 photocatalysis of the pharmaceutical propranolol: solar and artificial light. Applied Catalyst B. 2013;130-131:249–256. doi: 10.1016/j.apcatb.2012.10.003
[56] Fawei Z, Yu Y, Ping Z. Work function of single-wall silicon carbide nanotube. Appl Phys Lett. 2010;97:263105. doi: 10.1063/1.3532842
[57] Amir M, Mehdi D, Ali E. Nitrogen-doped (6,0) and (4,4) single-walled SiC nanotubes: a DFT study on surface reactivity and NMR parameters. Superlattices Microstruct. 2013;60:179–191.
[58] Ahmed M, Ahmed B. Magnetism of single-walled silicon carbide nanotubes doped by boron, nitrogen and oxygen. J Magn Magn Mater. 2012;324:2753–2760. doi:10.1016/j.jmmm.2012.04.003
[59] Ram SS, Ankit S. Hydrogen adsorption in metal-decorated silicon carbide nanotubes. Chem Phys Lett. 2016;660:155–159. doi:10.1016/j.cplett.2016.08.021
[60] Ploysongsri N, Vchirawongkwin V, Ruangpornvisuti V. Hydrogen boride nanotubes and their C, N, O decoration and doping derivatives as materials for hydrogen-containing gases storage and sensing: a SCC–DFTB study. Vacuum. 2021;187:110140. doi: 10.1016/j.vacuum.2021.110140
[61] Singh RS. CO2 capture by metal-decorated silicon carbide nanotubes. Silicon. 2023;2023:02368–9. doi: 10.1007/s12633-023-02368-9
[62] Acosta-Herazo R, Mueses MÁ, Puma GL, et al. Impact of photocatalyst optical properties on the efficiency of solar photocatalytic reactors rationalized by

the concepts of initial rate of photon absorption (IRPA) dimensionless boundary layer of photon absorption and apparent optical thickness. Chem Eng J. 2019;356:839–849.
[63] Romero V, De la Cruz N, Dantas RF, et al. Photocatalytic treatment of metoprolol and propranolol. CatalToday. 2011;161:115–120. doi: 10.1016/j.cattod.2010.09.026
[64] Pereira Cavalcante R, Falcao Dantas R, Bayarri B, et al. Photocatalytic mechanism of metoprolol oxidation by photocatalysts TiO2 and TiO2 doped with 5% B: primary active species and intermediates. Appl Catal B Environ. 2016;194:111–122. doi: 10.1016/j.apcatb.2016.04.054
[65] Raveendran A, Chandran M, Dhanusuraman R. A comprehensive review on the electrochemical parameters and recent material development of electrochemical water splitting electrocatalysts. RSC Adv. 2023;13(6):3843–3876. doi: 10.1039/D2RA07642J